PROCEEDINGS A

rspa.royalsocietypublishing.org

Research

Article submitted to journal

Subject Areas:
computational biology, biochemistry, mathematical modelling and simulation

Keywords:
chemical reaction networks, enzymes, posttranslational modifications, reaction kinetics, positive autoregulation

Author for correspondence:
R. P. Araujo
e-mail: r.araujo@qut.edu.au

Ultrasensitivity and bistability in covalent modification cycles with positive autoregulation

C. Jeynes-Smith[1,2] and R. P. Araujo[1,2]

[1]School of Mathematical Sciences, Queensland University of Technology, Brisbane, Australia.
[2]Institute of Health and Biomedical Innovation (IHBI), Brisbane, Australia.

Switch-like behaviours in biochemical networks are of fundamental significance in biological signal processing, and exist as two distinct types: ultrasensitivity and bistability. Here we propose two new models of a reversible covalent-modification cycle with positive autoregulation (PAR) - a motif structure that is thought to be capable of both ultrasensitivity and bistability in different parameter regimes. These new models appeal to a modelling framework that we call *complex complete*, which accounts fully for the molecular complexities of the underlying signalling mechanisms. Each of the two new models encodes a specific molecular mechanism for PAR. We demonstrate that the modelling simplifications for PAR models that have been used in previous work, which rely on a Michaelian approximation for the enzyme-mediated reactions, are unable to accurately recapitulate the qualitative signalling responses supported by our 'full' complex-complete models. Strikingly, we show that the parameter regimes in which ultrasensitivity and bistability obtain in the complex-complete framework contradict the predictions made by the Michaelian simplification. Our results highlight the critical importance of accurately representing the molecular details of biochemical signalling mechanisms, and strongly suggest that the Michaelian approximation may be inadequate for predictive models of enzyme-mediated chemical reactions with added regulations.

© The Authors. Published by the Royal Society under the terms of the Creative Commons Attribution License http://creativecommons.org/licenses/by/4.0/, which permits unrestricted use, provided the original author and source are credited.

THE ROYAL SOCIETY PUBLISHING

1. Introduction

The capacity for collections of biochemical reactions to respond in a switch-like, or *all-or-none*, manner is of fundamental significance in biological signal processing, and has been widely observed in many different signalling contexts [1–3]. Biochemical switch-like responses can exist as two distinct types [4,5]: ultrasensitivity, which is a steeply sigmoidal, monostable, dose-response profile; and bistability, a commonly-observed form of multistationarity, which constrains the system to exist in one of two possible stable steady-states for a given level of stimulus.

Ultrasensitivity has been implicated in functionally important switching mechanisms across a wide variety of biological contexts, ranging from cell signalling pathways [6,7], budding in yeast [8,9], maturation of xenopus oocytes [10,11], and embryonic differentiation [12]. More recently, ultrasensitivity has been recognised as an essential component in many robust perfect adaptation (RPA) mechanisms [13–15]. RPA is the ability of a system to asymptotically track a fixed 'set-point' following persistent perturbations to its interacting elements. This keystone signalling response is thought to be an essential characteristic of all evolvable and self-regulating biosystems [14,15], and has been ubiquitiously observed across all levels of biological organisation, from chemotaxis in single-celled organisms [16–27], to complex sensory systems [28–38]. Importantly, the dysregulation of RPA is believed to be linked to disorders such as cancer progression, drug addiction, chronic pain, and metabolic syndrome [39–44].

While the history of mathematical approaches to the study of ultrasensitivity-generating mechanisms may be traced back to the work of AV Hill [45] on cooperative binding in haemoglobin, the seminal work of Goldbeter and Koshland [46] on *zero-order* ultrasensitivity has exerted a profound influence on our modern understanding of ultrasensitivity. Indeed, it was Goldbeter and Koshland [46] who formally defined an ultrasensitive response as 'an output response that is more sensitive to change in stimulus than the hyperbolic (Michaelis-Menten) equation'. Their landmark findings demonstrated that enzyme-mediated covalent modification cycles (such as phosphorylation/dephosphorylation cycles, or methylation/demethylation cycles, for instance) are capable of generating sensitivities comparable to cooperative enzymes with high Hill coefficients when the interconverting enzymes operate in their 'zero-order' regions (ie. in the region of saturation with respect to their protein substrates). Importantly, this was the first known example of *unlimited* ultrasensitivity: unlike the response of cooperative enzymes, where the steepness of the dose-response profile was limited, the zero-order mechanism allowed steepness to be increased indefinitely by 'tuning' certain parameter groups. More recently, a number of additional ultrasensitivity-generating mechanisms have been identified [47, 48], including inhibitor-generated ultrasensivity and substrate competition [48–51], cooperative binding [52,53], positive feedback [3,6,54], multisite phosphorylation [9,12,55], and negative feedback [8,48]. Some mathematical models also support the idea that cascade structures can promote ultrasensitivity [11].

In contrast to ultrasensitivity, bistability gives rise to a discontinuous switching mechanism. Bistability is widely believed to play a vital functional role in gene regulatory networks [56–60], cell differentiation [61,62], cell-cycle regulation [63,64], lineage commitment during development [2], exit from quiescence in mammalian cells [65], and biochemical and working memory [66,67]. Moreover, a bistable switch can exist as a one-way (irreversible) switch, or a two-way ('toggle') switch. Toggle switches are reversible but exhibit hysteresis, whereby once the switch has been 'tripped' by a suitable increase in stimulus, propelling the system to its upper steady-state, a *much larger decrease* in input stimulus is required to bring the system back down to its lower steady-state - a functionally important response in the context of fluctuating inputs [2,66,68]. One-way switches, on the other hand, can never return the system to its lower steady-state once the switch has been tripped. The aberrant formation of such one-way switches is thought to play a particularly pernicious role in cancer signalling dysregulation, by driving the constitutive activation of oncoproteins [5,69,70]. Mathematically, bistability is thought to arise from a variety of

underlying mechanisms, including: positive autoregulation (PAR) and positive feedback, where a molecule either directly or indirectly promotes its own creation [56,57,59,65,66,71–73]; cooperative binding, where the binding of one molecule enhances the binding of subsequent molecules [63,74], antagonism, where one molecule benefits at the loss to another [62,75], and double negative feedback, a cycle in which two interacting molecules mutually inhibit each other [73].

Although emergent network behaviours such as bistability and ultrasensitivity, and the related phenomenon of RPA, have been the focus of many mathematical models, the detailed molecular mechanisms that might support these functions in 'real', highly complex signalling networks are yet to be understood. Indeed, a frontier research problem in biochemical signalling is the question of how specialised signal processing functions such as ultrasensitivity are implemented at the *microscale* of complex networks, through the highly intricate interactions of collections of proteins [15]. Even small collections of relatively simple enzyme-mediated reactions can involve the formation of a number of transient, intermediate molecular states, and can quickly give rise to complicated mathematical descriptions when all such states are explicitly accounted for. As a consequence, mathematical models of biochemical signal processing to date have typically been highly simplified - either by neglecting many of the proteins known to be involved, and frequently by simplifying the mathematical nature of their interactions - most notably through the (often indiscriminate) use of the Michaelis-Menten equation, involving the quasi-steady-state assumption (QSSA) on intermediate protein-protein complexes. Well-established and influential models of RPA in particular, have relied on such Michaelian descriptions of protein-protein interactions to suggest that specific parameter regimes promote robust adaptation by conferring ultrasensitivity at certain embedded 'nodes' of the network. The three-node RPA models published by Ma et al. [13], in particular, suggest that Michaelian models of positive autoregulation (PAR) are supportive of ultrasensitivity, and hence RPA, in very specific parameter regimes. But to what extent might these responses still be realized in more complex but realistic signalling descriptions, which account for all intermolecular interactions and intermediate protein-protein complexes?

In the present paper, we attempt to offer important new insights into this vitally important question. We propose several new, simple, yet detailed, mathematical models of covalent modification cycles incorporating PAR, appealing to a mathematical framework we call *complex-complete*. In this *complex-complete* framework, the molecular details of each specific PAR mechanism will be considered explicitly, and all intermediate protein-protein complexes accounted for. We will consider the capacity of each such model to exhibit bistability and ultrasensitivity, through model simulations over a wide range of parameters, and compare these outcomes to the behaviour supported by the well-established Michaelian model of PAR [13].

As a backdrop to these novel complex-complete models of PAR, we first briefly review the two main classes of simplified frameworks for the mathematical modelling of covalent modification cycles: simplified mass-action models, and Michaelian models (Fig 1).

(a) Simplified models of covalent modification cycles

Simplified mass-action models exclude intermediate protein-protein complexes (see Fig 1b). A simplified mass-action model of a covalent-modification cycle thus produces a single ordinary differential equation (ODE) for the output $W^*(t)$, as in Eq (1.1),

$$\frac{dW^*}{dt} = k_1 E_{1tot}(W_{tot} - W^*) - k_2 E_{2tot} W^*, \tag{1.1}$$

with

$$W_{tot} = W + W^* \tag{1.2}$$

as a *conservation relation*, yielding the concentration of the unmodified protein, $W(t)$, once $W^*(t)$ is known from (1.1).

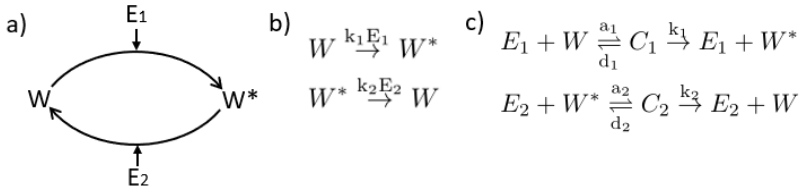

Figure 1. A mathematical framework for the modelling of a single covalent-modification cycle (a) A schematic representation of a reversible covalent-modification cycle in which a protein substrate (W) is chemically modified by an enzyme, E_1, into an active form (W^*). The active form is, in turn, converted back to its unmodified form through the action of a second, independent, enzyme, E_2. These processes may then be realised as a chemical reaction mechanism (b and c), with a corresponding graph structure, from which rate equations (ODEs) are 'induced' [76]. (b) A 'complex-free' mechanism, in which enzyme concentrations are incorporated into the biochemical rate constants (k_1, k_2) can be used as the basis of a simplified mass-action model of the cycle. (c) A reaction mechanism that explicitly includes transient enzyme-substrate complexes (C_1, C_2) can be used as the basis of either a *complex-complete* mass action model, or a Michaelian model. The Michaelian model is a simplification of the complex-complete framework, whereby complexes are assumed to reach a steady-state on a much faster time-scale than the other processes in the reaction, and whose steady-state concentrations are assumed to be negligible.

By contrast, Michaelis-Menten kinetics do take into account the existence of intermediate complexes in the system (see Fig 1c), but their explicit consideration is avoided through the application of the quasi steady-state assumption (QSSA). By the QSSA, complex association (a_i) and dissociation (d_i) processes are assumed to occur on a significantly faster timescale than the catalysis (k_i) reaction. Moreover, the steady-state concentrations of the complexes (there being two enzyme-substrate complexes, C_1 and C_2, in a single covalent-modification cycle), having rapidly been reached, are assumed to be negligible in comparison with the total protein concentration (ie. $W_{tot} = W^* + W + C_1 + C_2 \approx W^* + W$). We thereby obtain a single equation for $W^*(t)$ (Eq (1.3)), which features parameter groups known as Michaelis constants, $K_1 = \frac{d_1+k_1}{a_1}$ and $K_2 = \frac{d_2+k_2}{a_2}$,

$$\frac{dW^*}{dt} = \frac{k_1 E_{1tot}(W_{tot} - W^*)}{K_1 + W_{tot} - W^*} - \frac{k_2 E_{2tot} W^*}{K_2 + W^*}. \tag{1.3}$$

The first of the following conservation relations

$$\begin{aligned} W_{tot} &\approx W + W^*, \\ E_{1tot} &= E_1 + C_1 \approx E_1, \\ E_{2tot} &= E_2 + C_2 \approx E_2, \end{aligned} \tag{1.4}$$

determines the concentration of $W(t)$ once $W^*(t)$ is established from (1.3).

We refer to models that consider all signalling events and intermediate molecules explicitly, thus providing a detailed representation of the signalling mechanisms, as *complex-complete mass-action models*. The complex-complete mass-action model associated with the chemical reaction

network in Fig 1c can be expressed as a system of four ODEs and three conservation equations,

$$\begin{aligned}\frac{dW}{dt} &= d_1C_1 + k_2C_2 - a_1SWE_1,\\ \frac{dW^*}{dt} &= d_2C_2 + k_1C_1 - a_2W^*E_2,\\ \frac{dC_1}{dt} &= a_1WE_1 - d_1C_1 - k_1C_1,\\ \frac{dC_2}{dt} &= a_2W^*E_2 - d_2C_2 - k_2C_2,\end{aligned} \tag{1.5}$$

and

$$\begin{aligned}W_{tot} &= W + W^* + C_1 + C_2,\\ E_{1tot} &= E_1 + C_1,\\ E_{2tot} &= E_2 + C_2.\end{aligned} \tag{1.6}$$

As mathematical models grow in size and complexity, simplified mass-action and Michaelian descriptions of the various components of the system can significantly reduce the number of variables and parameters to be considered. On the other hand, these benefits come at the expense of neglecting signalling events which could potentially alter the qualitative nature of the systems response in significant ways ([15,75,77]). Importantly, Goldbeter and Koshland's seminal work on zero-order ultrasensitivity [46] has suggested that the Michaelian model of a covalent modification cycle, Eq (1.3), provides a good approximation to the ultrasensitive behaviour of the complex-complete mass-action model *provided* that $E_{1tot}, E_{2tot} \ll W_{tot}$ - a parametric condition unlikely to obtain in many signal transduction networks, or other highly complex bionetworks in nature [14]. Moreover, if additional regulations such as autoregulatory interactions are present in the system, with an inevitable increase in the number of intermediate protein-protein complexes, it is unclear if simplified Michaelian descriptions of the system would be capable of recapitulating the qualitative behaviours of the corresponding complex-complete models for *any* parameter regime.

Although the larger number of variables and parameters often necessitates numerical, rather than analytical, approaches, these models allow the complexity of the system to speak for itself, and can be used to verify the extent to which simplified models of signalling motifs can recapitulate the behaviours of more detailed, accurate and mechanistic mathematical descriptions.

We now proceed to compare three different models of a covalent-modification cycle with positive autoregulation (PAR) - the well-established Michaelian model studied by Ma et al. [13], along with two novel complex-complete mass-action models.

(b) A Michaelian Model of Positive Autoregulation (PAR)

In order to generate ultrasensitivity (and hence RPA when suitably embedded into an appropriate network topology) via positive autoregulation (PAR) of a covalent modification cycle, Ma et al. [13] used an equation of the following form:

$$\frac{dW^*}{dt} = \frac{k_1E_1W^*(W_{tot} - W^*)}{K_1 + (W_{tot} - W^*)} - \frac{k_2E_2W^*}{K_2 + W^*}. \tag{1.7}$$

Here PAR has been incorporated into a Michaelian model by assuming that the rate of increase of W^* occurs in direct proportion to E_1W^* (rather than just E_1, as is the case for the Michaelian model without added regulations), thereby enabling the output molecule to enhance its own production. It is clear from the form of Eq(1.7) that if $K_1 \ll W_{tot} - W^*$ and $K_2 \gg W^*$, then at steady state, $0 \approx W^*(k_1E_1 - k_2E_2/K_2)$. Thus, the system can exhibit unlimited ultrasensitivity as this parametric limit is approached, with a near-vertical dose-response occurring at $E_{1tot} \approx E_1 = \frac{k_2}{k_1K_2}E_2$.

In Fig 2 we examine how the Michaelis constants of this system are the key drivers of both bistability and (unlimited) ultrasensitivity in this model. In particular, for an initial choice of $K_1 \approx K_2 \approx 1$, the rate of increase in W* (orange/black lines), as given by the first term in Eq(1.7), intersects the rate of decrease (blue dashed line) in multiple places, indicating the existence of multiple steady states (bistability, in this case) for some values of E_1. As we increase the value of K_2 and decrease K_1, we observe a narrowing in the range of values of E_1 for which bistability obtains. This occurs as the negative rate of change approaches the same form as the positive rate of change. For $K_1 \ll W_{tot} - W^*$ and $K_2 \gg W^*$, the two curves approach an exact match, and complete overlap, for $E_1 = \frac{k_2}{k_1 K_2} E_2$. Under these conditions, every non-zero value of W^* is compatible with a steady state at $E_1 = \frac{k_2}{k_1 K_2} E_2$ - a scenario that corresponds to unlimited ultrasensivity (ie. a vertical dose-response curve at the noted value of E_1).

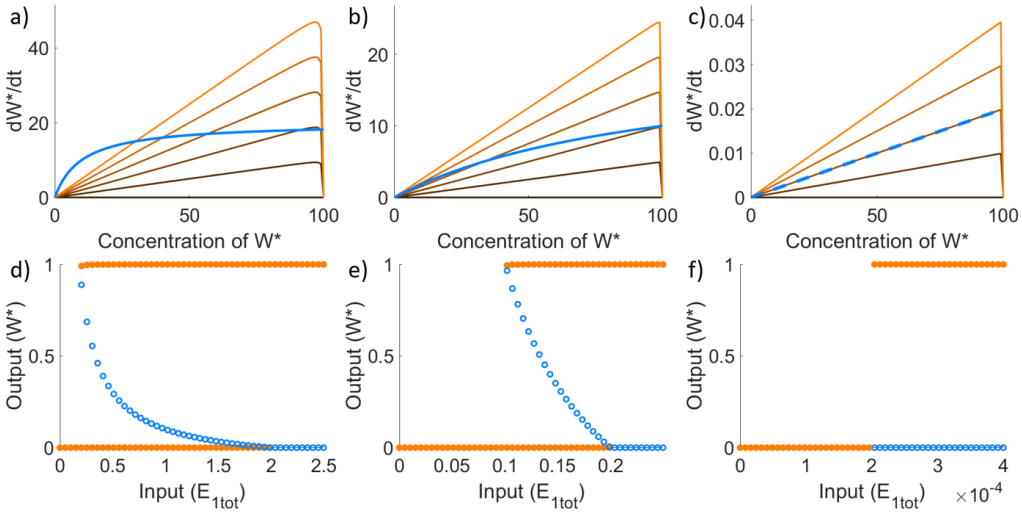

Figure 2. Bistability and Ultrasensitivity in a Michaelian model of PAR The Michaelian model of PAR (Eq (1.7)) can exhibit both bistability, as a two-way (toggle) switch (a, b, d, e), and unlimited ultrasensitivity (c, f), depending on model parameters. Figures (a-c) plot the positive and negative contributions of the rate of change in W^* from Eq (1.7), for three different parameter sets. In each case, the negative component (independent of E_1) is represented by the blue line. Since the positive component is a function of E_1 (the input), we represent the positive component of the rate change by the solid line which changes from black to orange with an increasing value of E_1. The intersection of the positive and negative components thus indicates the steady states of the system, which are plotted in (d-f), respectively, for a range values of E_1. Stable steady states are represented by solid circles, with unstable states represented by open circles. As shown, figures (a) and (b) have multiple intersection points for certain values of E_1. These existence of multiple steady states is highlighted by the bistable plots in the corresponding figures (d) and (e). Parameters: all six plots use $k_1 = k_2 = 1$, $W_{tot} = 100$, $E_2 = 20$. In addition, (a) and (d) use: $K_1 = 10^{-1}$ and $K_2 = 10^1$; (b) and (e) use: $K_1 = 10^{-2}$ and $K_2 = 10^2$; and (c) and (e) use: $K_1 = 10^{-5}$ and $K_2 = 10^5$.

Note that in the Michaelian model of PAR by Ma et al. [13], there is no consideration of *how* the output molecule W^* might upregulate its own production through its interactions with other molecules, and thus no accounting for any particular autoregulatory *mechanism*. As a consequence, there is no way to determine how well this model might reflect PAR mechanisms in 'real' biochemical reaction networks. In order to consider the role of the *mechanism* in PAR, we propose two possible chemical reaction mechanisms - a direct positive autoregulatory mechanism (hereafter, PAR-d), and an indirect mechanism (hereafter, PAR-i).

(c) A novel model of Direct Positive Autoregulation (PAR-d)

In order implement a direct PAR mechanism we supplement the basic covalent-modification cycle (Fig 1c) to include a third set of reactions whereby the output, W^*, binds in trans to the unmodified protein W, thereby catalysing the conversion of the latter to W^*. In the process of doing so, an intermediate protein-protein complex comprising both W and W^* is formed. We represent this process schematically in Fig 3a and by the chemical reaction network in Fig 3b.

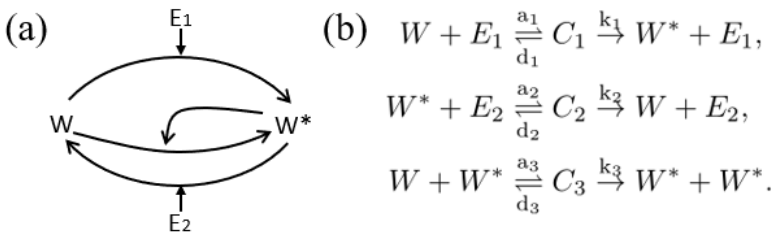

Figure 3. PAR-d System (a) Schematic representation of the PAR-d mechanism. (b) Chemical reaction network corresponding to the PAR-d mechanism, comprising three groups of reactions: (i) E_1 binding reversibly to W, forming a complex C_1, and catalysing the production of W^* from W; (ii) E_2 binding reversibly to W^*, forming a complex C_2, and catalysing the production of W from W^*; and (iii) W^* binding reversibly to W, forming a complex C_3, and catalysing the conversion of W to W^*.

This chemical reaction network, through the law of mass action, induces the following system of ordinary differential equations:

$$\frac{dW}{dt} = d_1C_1 + d_3C_3 + k_2C_2 - a_1WE_1 - a_3WW^*, \tag{1.8}$$

$$\frac{dW^*}{dt} = d_2C_2 + d_3C_3 + k_1C_1 + 2k_3C_3 - a_2W^*E_2 - a_3WW^*, \tag{1.9}$$

$$\frac{dE_1}{dt} = d_1C_1 + k_1C_1 - a_1WE_1, \tag{1.10}$$

$$\frac{dE_2}{dt} = d_2C_2 + k_2C_2 - a_2W^*E_2, \tag{1.11}$$

$$\frac{dC_1}{dt} = a_1WE_1 - d_1C_1 - k_1C_1, \tag{1.12}$$

$$\frac{dC_2}{dt} = a_2W^*E_2 - d_2C_2 - k_2C_2, \tag{1.13}$$

$$\frac{dC_3}{dt} = a_3WW^* - d_3C_3 - k_3C_3. \tag{1.14}$$

The summation of Eqs (1.8), (1.9), (1.12), (1.13), and (1.14) yields a conservation equation for the substrate protein,

$$W_{tot} = W + W^* + C_1 + C_2 + C_3. \tag{1.15}$$

Likewise, summation of Eqs (1.10), and (1.12), and of Eqs (1.11), and (1.13), yield conservation equations for the two enzymes:

$$E_{1tot} = E_1 + C_1, \tag{1.16}$$

$$E_{2tot} = E_2 + C_2. \tag{1.17}$$

(d) A novel model of Indirect Positive Autoregulation (PAR-i)

For the indirect implementation of PAR we introduce two new reaction groups to the reversible covalent-modification cycle. First, we add a reaction in which the output, W^*, can bind reversibly with the enzyme, E_1, forming the transient complex C_3. Then, in a second reaction group, the complex C_3 can bind reversibly to W, forming another complex C_4, which catalyses the conversion of W to W^*. In this way, the binding of W^* to E_1 (producing C_3) alters the efficiency of the enzyme E_1 through an allosteric interaction. Thus, in contrast to PAR-d, where W^* catalyses its own production from the unmodified form W, W^* now enhances its own production through an indirect mechanism, through its interactions with E_1. We illustrate the PAR-i mechanism by the schematic in Fig 4a, and produce a corresponding chemical reaction network in Fig 4b.

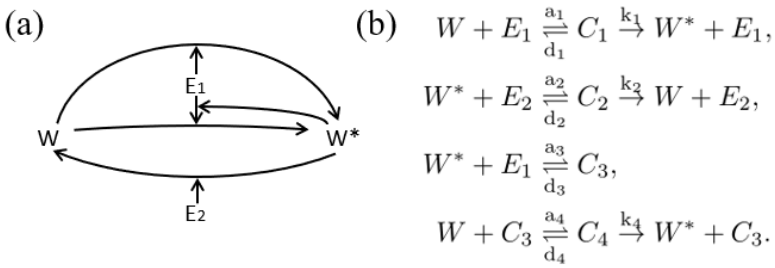

Figure 4. PAR-i System (a) Schematic representation of the PAR-i mechanism. b) A chemical reaction network for PAR-i. This includes four reaction groups: (i) E_1 binding reversibly to W, forming a complex C_1, and catalysing the production of W^* from W; (ii) E_2 binding reversibly to W^* forming a complex C_2, and catalysing the production of W from W^*; (iii) W^* binding reversibly with E_1 to form a complex C_3; and (iv) C_3 (containing enzyme E_1) binding reversibly with W, forming a complex C_4, catalysing the conversion of W to W^*.

By the Law of Mass-action, we obtain a system of ordinary differential equations from the chemical reaction network in Fig 4b:

$$\frac{dW}{dt} = d_1C_1 + k_2C_2 + d_4C_4 - a_1WE_1 - a_4WC_3, \tag{1.18}$$

$$\frac{dW^*}{dt} = k_1C_1 + d_2C_2 + d_3C_3 + k_4C_4 - a_2W^*E_2 - a_3W^*E_1, \tag{1.19}$$

$$\frac{dE_1}{dt} = d_1C_1 + k_1C_1 + d_3C_3 - a_1WE_1 - a_3W^*E_1, \tag{1.20}$$

$$\frac{dE_2}{dt} = d_2C_2 + k_2C_2 - a_2W^*E_2, \tag{1.21}$$

$$\frac{dC_1}{dt} = a_1WE_1 - d_1C_1 - k_1C_1, \tag{1.22}$$

$$\frac{dC_2}{dt} = a_2W^*E_2 - d_2C_2 - k_2C_2, \tag{1.23}$$

$$\frac{dC_3}{dt} = a_3W^*E_1 + d_4C_4 + k_4C_4 - d_3C_3 - a_4WC_3, \tag{1.24}$$

$$\frac{dC_4}{dt} = a_4WC_3 - d_4C_4 - k_4C_4, \tag{1.25}$$

The summation of Eqs (1.18), (1.19), (1.22), (1.23), (1.24), and (1.25) gives a conservation equation for the substrate protein,

$$W_{tot} = W + W^* + C_1 + C_2 + C_3 + 2C_4. \tag{1.26}$$

Similarly, the summation of Eqs (1.20), (1.22), (1.24), and (1.25), and of Eqs (1.21) and (1.23), yield conservation equations for the two interconverting enzymes:

$$E_{1tot} = E_1 + C_1 + C_3 + C_4, \tag{1.27}$$

$$E_{2tot} = E_2 + C_2. \tag{1.28}$$

2. Results

We have undertaken extensive numerical explorations of the dose-response profiles of our two new complex-complete models of PAR, examining how the steady-state concentration of the output (W^*) changes with the input (E_{1tot}). In all figures we show W^* as a proportion of the total substrate protein available in the system (W_{tot}). These simulations consider the qualitative influence of each individual rate constant (a_i, d_i, k_i), the total protein abundances (W_{tot} and E_{2tot}, considered constants) as well as key parameter groups - the Michaelis constants (K_1, K_2, K_3), and the dissociation constant (K_d) that occurs in PAR-i. Each parameter, or parameter group, is varied in turn over the range (10^{-10}, 10^{10}) while holding all other parameters fixed. Linear stability analysis is used to classify the stability of all steady-states.

Our overarching goal is to determine the extent to which bistability (as a one-way switch and/or as a toggle switch) and ultrasensitivity are obtained in our complex-complete models of PAR, and to establish the similarities and differences in the predictions of these detailed models in comparison with the simpler Michaelian model of PAR.

(a) PAR-d readily exhibits bistability and can create both one-way and two-way switches

Our extensive computational simulations reveal that the PAR-d model is highly prone to bistability. Indeed, whenever a monostable profile was obtained, almost any attempt to further increase the sensitivity (steepness of the slope) of the dose-response curve by increasing (or decreasing) a suitable parameter ultimately led to the onset of bistability.

Strikingly, the existence of bistability in the dose-response of PAR-d differs from that in the simple Michaelian model in a number of fundamental ways. First, unlike the Michaelian model which only admits two-way (toggle) switches in its bistable regime, PAR-d also has the potential for one-way (irreversible) switches. In Fig 5 we demonstrate how altering a single parameter can shift the system's response from monostable ultrasensitivity, to a bistable two-way switch, to a bistable one-way switch.

Furthermore it is intriguing to observe that, in stark contrast to the Michaelian model, the capacity for bistability in PAR-d is *not* determined by the Michaelis constants alone. In Fig 5, for instance, a full range of behaviours is obtained from the model - from a monostable ultrasensitive profile, through to both one- and two-way switches - all generated with a single set of Michaelis constants K_1, K_2, K_3. In fact, for each of the three individual rate constants, a_i, d_i, k_i that comprise a Michaelis constant, K_i, we discovered that it is the catalytic constant, k_i, specifically, that controls the qualitative response of the system and the shape of its dose-response profile.

We explore this finding further in Fig 6, where we examine the various possible combinations of holding a Michaelis constant fixed, along with *one* of its component rate constants, while varying the two remaining rate constants. In Fig 6a, we hold K_1 and k_1 constant, while increasing d_1 and a_1 in a proportion that maintains the constant K_1. The profiles that are generated with these changes are all identical. By contrast, when we alter k_1 and a_1 (Fig 6b) and k_1 and d_1 (Fig 6c) we observe clear differences amongst the profiles. We also observe that across Fig 6b and Fig 6c, dose-response profiles associated with the matching values of K_1 and k_1 are the same irrespective of the value of a_1 and d_1. These same behaviours can be observed in the second (Fig 6d-f) and third (Fig 6g-i) reactions.

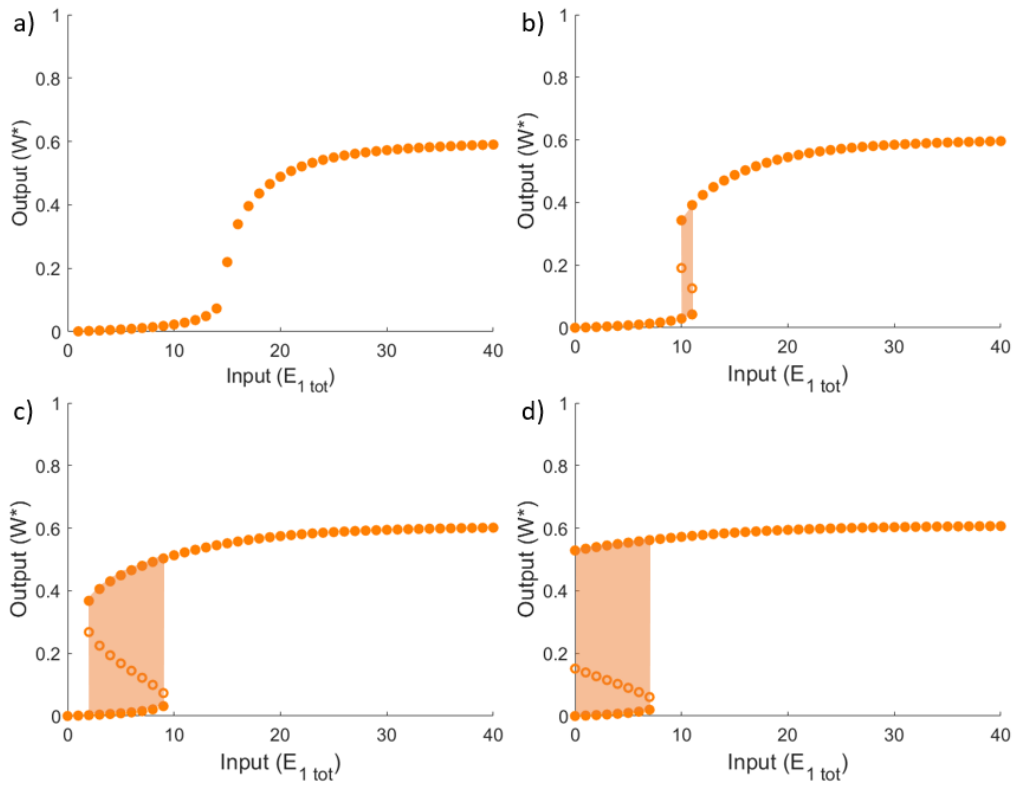

Figure 5. Bistability in PAR-d Analysis of PAR-d dose-response profiles for (a) a continuous, ultrasensitive regime, (b) a regime corresponding to a very narrow bistable regions, just past the bifurcation point that separates ultrasensitivity from bistability, (c) a bistable regime with a two-way switch, and (d) a bistable regime with a one-way switch. Solid circles denote stable solutions, while open circles denote unstable solutions. The shaded areas highlight the bistable regions. Parameters: All plots use $W_{tot} = 100$, $E_{2tot} = 20$, $a_1 = d_1 = k_1 = a_2 = d_2 = k_2 = 1$. The different profiles vary in the rate constants a_3, d_3, and k_3: (a) $a_3 = 0.01$, and $d_3 = k_3 = 1$; (b) $a_3 = 0.02$, and $d_3 = k_3 = 2$; (c) $a_3 = 0.03$, and $d_3 = k_3 = 3$ and d) $a_3 = 0.04$, and $d_3 = k_3 = 4$.

In fact, it is clear that the catalytic constants (k_i) play a unique and important role in tuning the shape of the system's dose-response profiles. In Figs 5 and 6, the parameters are altered to increase the catalytic constant in question without also altering the corresponding Michaelis constant. On the other hand, by increasing k_1 on its own, and hence increasing K_1 simultaneously, the system changes from monostable ultrasensitivity, to bistability, and then back to monostable ultrasensitivity (see Fig 7) - an unusual and unexpected behaviour not afforded by the simple Michaelian model. Remarkably, the monostable regions of these profiles continue to increase in sensitivity, as this complex phenomenon unfolds, despite the inclusion of the bistable region. This behaviour is tied uniquely and specifically to the first catalytic constant, k_1.

Moreover, while PAR-d can exhibit ultrasensitivity as demonstrated in Figs 6 and 7, the steepness of this near-vertical region of the dose-response cannot be increased indefinitely - in marked contradistinction to the Michaelian model which supports ulimited ultrasensitivity. As shown in Fig 7, increasing k_1 can increase the sensitivity of the dose-response profile, but the steepness that can be achieved is limited. In addition, the location of the ultrasensitive portion of the curve is consistently moved to the left, towards the origin, which also constrains the development of ultrasensitivity due to this particular parameter change. In Fig 8, decreasing K_1 with fixed k_1 highlights the limit in ultrasensitivity that is approached as K_1 is reduced.

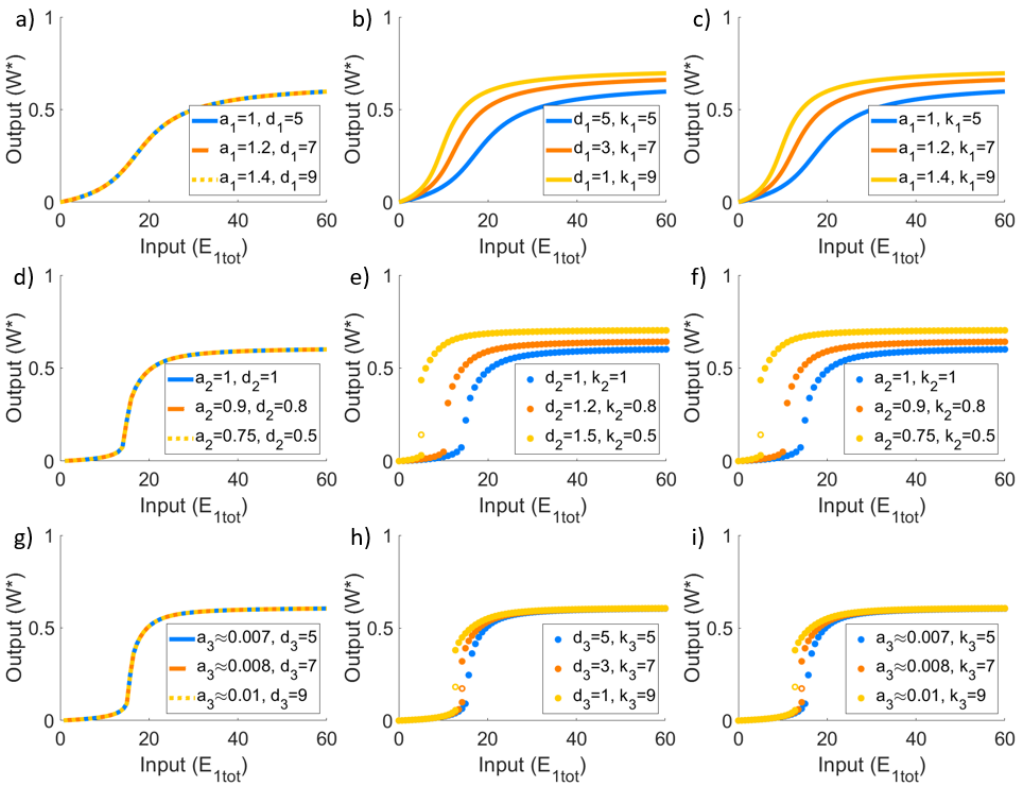

Figure 6. Varying rate constants in PAR-d Pairs of independent rate constants are altered whilst holding the corresponding values of K_1, K_2, and K_3 fixed. In (a), (d), (g) we find that holding the catalytic constant fixed results in no changes to the dose-response profile. Parameters: $W_{tot} = 100$ and $E_{2tot} = 20$ for all plots. For (a)-(c): $a_1 = a_2 = d_3 = k_3 = 1$, $d_1 = k_1 = d_2 = k_2 = 5$, $a_3 = 0.01$; for (d)-(f): $a_1 = d_1 = k_1 = a_2 = d_2 = k_2 = d_3 = k_3 = 1$, $a_3 = 0.01$; for (g)-(i): $a_1 = d_1 = k_1 = a_2 = d_2 = k_2 = 1$, $a_3 = 0.007$, and $d_3 = k_3 = 5$. Varied rate constants identified in the figure legends. Closed circles indicate stable steady-states; open circles are unstable steady-states.

Altering the other parameters of the PAR-d model (K_2, K_3, and W_{tot}), in an attempt to increase sensitivity, ultimately culminates in the onset of bistability. Unlike the situation illustrated in Fig 7, where the system switches from monostable to bistable and back to monostable for a monotone increase in a single parameter, bistability now persists once it is triggered at a critical value of the parameter in question. In particular, in Fig 9, we observe that decreasing K_2 increases the sensitivity in the lower half of the substrate profile, without greatly affecting the sensitivity in the upper half. This ultimately leads to bistability as the lower half is shifted too far to the right. Further decreases in K_2 do not lead to the creation of a one-way switch, as we illustrate by the profiles for $K_2 = 0.4$ and $K_2 = 0.2$ which can be observed to overlap without significant change.

For the parameters K_3 (Fig 10a) and W_{tot} (Fig 10b), on the other hand, continued monotone alterations in these parameters transform the two-way switch into a one-way switch. By either decreasing K_3 or increasing W_{tot}, the upper portion of the dose-response profile is shifted rapidly to the left, much more rapidly than the shifting of the lower portion, which leads to an overlap, creating bistability. This trend continues and ultimately leads to the creation of a one-way switch as the upper portion of the curve moves to the left past the location of the vertical axis.

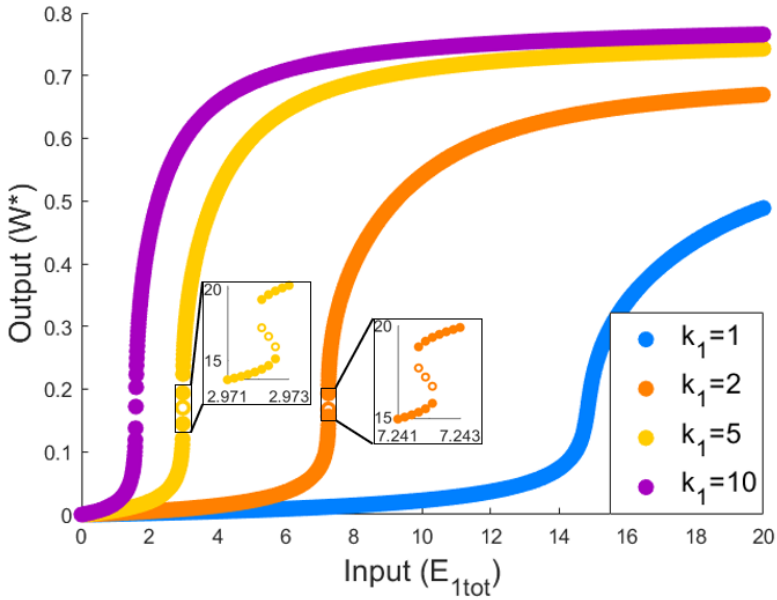

Figure 7. The role of the catalytic constant k_1 in PAR-d Increasing k_1 while holding all other biochemical rate constants fixed engenders a complex response in the system's dose-response profile. As illustrated here, continued increases in k_1 transform the dose-response profile from monostable, to bistable, and back to monostable, all the while increasing the sensitivity of the monostable regions. Parameters: $a_1 = d_1 = a_2 = d_2 = k_2 = d_3 = k_3 = 1$, and $a_3 = 0.01$, $W_{tot} = 100$, $E_{2tot} = 20$. Closed circles indicate stable steady-states; open circles are unstable steady-states.

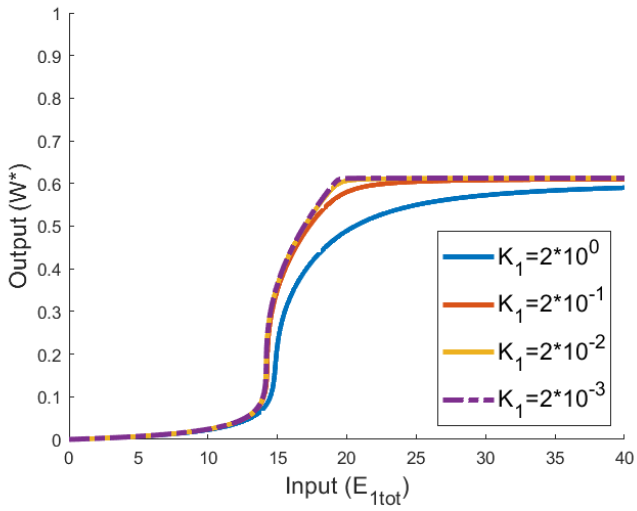

Figure 8. The role of Michaelis constant K_1 in PAR-d Here we decrease the value of K_1 by increasing the value of a_1 whilst holding d_1 and k_1 fixed. As shown, increasing K_1 increases sensitivity without giving rise to bistability, but cannot increase sensitivity indefinitely. Sensitivity is clearly observed to approach a limiting state. Parameters: $W_{tot} = 100$, $E_{2tot} = 20$, $d_1 = k_1 = a_2 = d_2 = k_2 = d_3 = k_3 = 1$, and $a_3 = 0.01$. To achieve the indicated values of K_1, we set $a_3 = 1$ (blue), $a_1 = 10$ (red), $a_1 = 100$ (yellow), and $a_1 = 1000$ (purple).

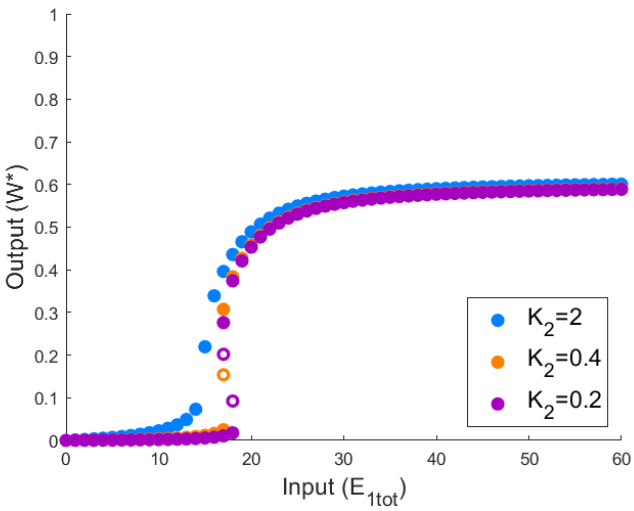

Figure 9. The role of Michaelis constant K_2 in PAR-d Here we alter the value of K_2, by altering the value of a_2 whilst holding d_2 and k_2 fixed. As shown, decreases in K_2 ultlimately lead to bistability, but can only create a two-way (not one-way) switch. Parameters: $W_{tot} = 100$, $E_{2tot} = 20$, $a_1 = d_1 = k_1 = d_2 = k_2 = d_3 = k_3 = 1$, and $a_3 = 0.01$. To achieve the indicated values of K_2, we set $a_2 = 1$ (blue), $a_2 = 5$ (orange), and $a_2 = 10$ (purple). Solid circles indicate stable steady-states; open circles indicate unstable steady-states.

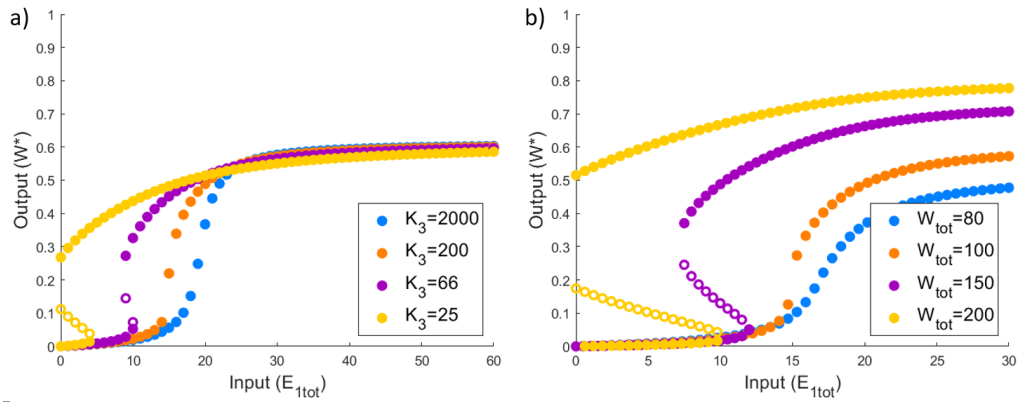

Figure 10. The role of Michaelis constant, K_3, and protein abundance, W_{tot}, in PAR-d Continued decreases in K_3, or increases in W_{tot} transform an initially monostable (ultrasensitive) profile into a bistable one, ultimately leading to the creation of a one-way switch. Parameters: $E_{2tot} = 20$, $a_1 = d_1 = k_1 = a_2 = d_2 = k_2 = d_3 = k_3 = 1$. (a) $W_{tot} = 100$, with $a_3 = 0.001$ (blue), $a_3 = 0.01$ (orange), $a_3 = 0.03$ (purple), and $a_3 = 0.08$ (yellow). (b) $a_3 = 0.01$, with $W_{tot} = 80$ (blue), $W_{tot} = 100$ (orange), $W_{tot} = 150$ (purple), and $W_{tot} = 200$ (yellow).

(b) PAR-i readily exhibits monostable responses but can produce two-way (*not* one-way) switches

Through extensive numerical simulations we find that PAR-i is tremendously less prone to bistability than the PAR-d model (which is highly prone to bistability) or the Michaelian model. Indeed, we find that the catalytic constant k_4 is the *only* parameter in this model that drives bistability (see Fig 11). This is a key distinction from the Michaelian model, wherein the two

Michaelis constants are the drivers of bistability, or the PAR-d model, where a number of parameters drive bistability as discussed in the previous section.

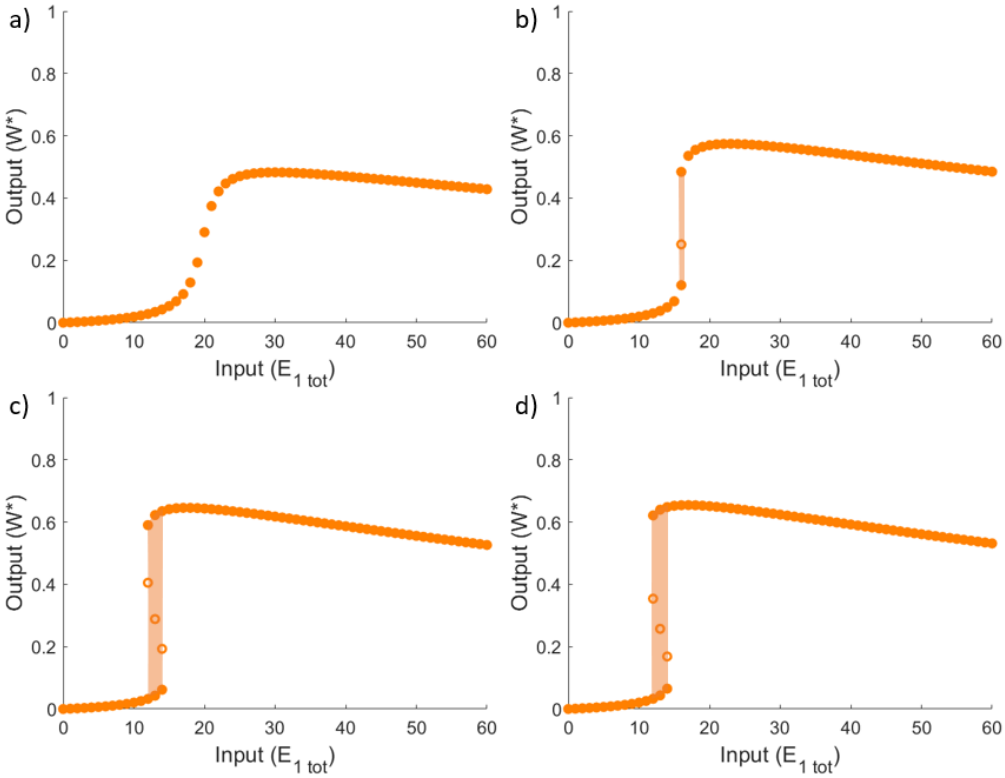

Figure 11. Bistability in PAR-i Analysis of steady-state solutions of PAR-i model for (a) a continuous, monostable, ultrasensitive regime, (b) a bistable regime which is very close to the bifurcation between continuous ultrasensitivity and bistability, and (c)-(d) bistable regimes with a two-way switch. solid circles indicate stable solutions, empty circles indicate unstable solutions. Shaded areas highlight bistable the region. Parameters: all plots use $W_{tot} = 100$, $E_{2tot} = 20$, $a_1 = a_2 = a_4 = d_1 = k_1 = d_2 = k_2 = d_4 = 1$, $d_3 = 10$, and $a_3 = 0.1$. The different profiles are created by increasing the rate constant k_4: (a) $k_4 = 1$; (b) $k_4 = 3$; (c) $k_4 = 30$; and (d) $k_4 = 300$.

The relationship between bistability and the parameter regime in the PAR-i model is quite subtle. In particular, while increasing the value of k_4 is able to convert a sensitive but monostable profile into a bistable one, it is striking to observe that many other parameters can *predispose* the system to bistability, enabling the bifurcation to occur at a lower value of k_4. In Fig 12, for instance, we show that for a given value of k_4, we are able to switch between ultrasensitivity and bistability by increasing the sensitivity of the system via a reduction in the Michaelis constants. In particular, decreasing the values of K_2 and K_4 increases the sensitivity of the underlying ultrasensitive monostable profile, allowing bistability to be triggered for smaller values of k_4. Interestingly, when K_1 is decreased, the system is 'pushed back' towards monostability. Nevertheless, Michaelis constants are not considered drivers of bistability in the sense that, for sufficiently low values of k_4, they are unable to achieve bistability on their own.

In common with the behaviour of PAR-d, we found that the catalytic constant, k_i, is the only component rate constant in each Michaelis constant, K_i, that exerts a qualitative influence on the shape of the system's dose-response profile. In Fig 13b, for instance, we see that decreasing k_2 increases the sensitivity of the profile, and may thereby predispose the system to bistability. On the

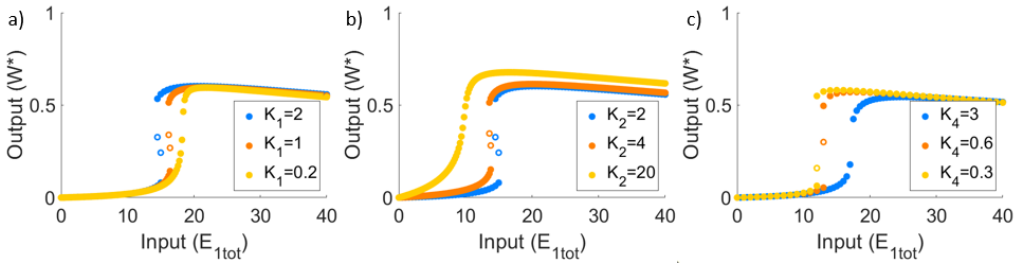

Figure 12. Michaelis constants can predispose PAR-i to bistability Altering the Michaelis constants for a given value of k_4 can take the system from monostability to bistability. Solid circles indicate stable solutions, while empty circles indicate unstable solutions. Parameters: all plots use $W_{tot} = 100$, $E_{2tot} = 20$, $a_1 = d_1 = k_1 = a_2 = d_2 = k_2 = a_4 = d_4 = 1$, $a_3 = 0.1$, and $d_3 = 10$. (a) $k_4 = 5$, $a_1 = 1$ (blue), $a_1 = 2$ (orange), and $a_1 = 10$ (yellow); (b) $k_4 = 5$, $a_2 = 1$ (blue), $a_2 = 0.5$ (orange), and $a_2 = 0.1$ (yellow); and (c) $k_4 = 2$, $a_4 = 1$ (blue), $a_4 = 5$ (orange), $a_4 = 10$. (yellow).

other hand, increasing k_1 increases sensitivity while also promoting monostability (see Fig 13a). In fact, we consistently found throughout our simulations that there is a very strong relationship between the values of k_1 and k_4, and the shape of the dose-response curve. In particular, for $k_1 = k_4$, this system is unable to achieve bistability, regardless of how the other parameters are altered.

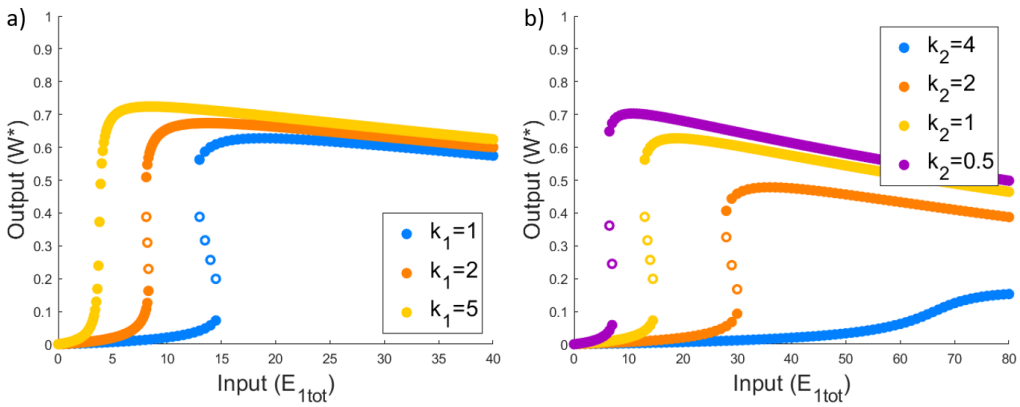

Figure 13. Low catalytic constants predispose PAR-i to bistability Reducing the catalytic constants k_1 and k_2, for a given value of k_4, can take the system from monostability to bistability. Solid circles indicate stable solutions and empty circles indicate unstable solutions. Parameters: $W_{tot} = 100$, $E_{2tot} = 20$, $a_1 = d_1 = k_1 = a_2 = d_2 = k_2 = a_4 = d_4 = 1$, $a_3 = 0.1$, $d_3 = 10$, and $k_4 = 10$. (a) $a_1 = d_1 = k_1 = 1$ (blue), $a_1 = d_1 = k_1 = 2$ (orange), $a_1 = d_1 = k_1 = 5$ (yellow); (b) $a_2 = d_2 = k_2 = 4$ (blue), $a_2 = d_2 = k_2 = 2$ (orange), $a_2 = d_2 = k_2 = 1$ (yellow), $a_2 = d_2 = k_2 = 0.5$ (purple).

As we show in Fig 14, increasing the total protein abundance, W_{tot} is also able to predispose the system to bistability.

Unlike the PAR-d model, but in common with the Michaelian model, PAR-i can only exhibit two-way (reversible) bistable switches, not one-way switches. As we illustrate in Fig 11, continued increases in the key parameter k_4 do not culminate a one-way switch. This is to be expected, of course, since when $E_{1tot} = 0$ for this particular PAR mechanism, there is no possibility of a 'forward' reaction in which W^* is created, and thus no opportunity for a non-zero steady-state in W^*.

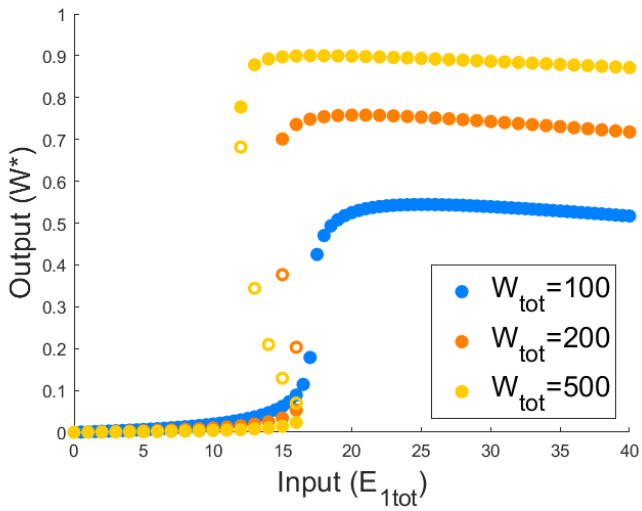

Figure 14. High total protein abundance predisposes PAR-i to bistability Increasing the total abundance of protein substrate, W_{tot}, for a given value of k_4, can take the system from monostability to bistability. Solid circles indicate stable solutions and empty circles indicate unstable solutions. Parameters: $E_{2tot} = 20$, $a_1 = d_1 = k_1 = a_2 = d_2 = k_2 = a_4 = d_4 = 1$, $a_3 = 0.1$, $d_3 = 10$, and $k_4 = 2$. We then set $W_{tot} = 100$ (blue), $W_{tot} = 200$ (orange), and $W_{tot} = 500$ (yellow).

A further notable distinction between PAR-i and both the Michaelian and PAR-d models is the eventual decrease in system output with continued increases in input (E_{1tot}). By analysing the abundances of intermediate complexes in this scenario, we find that after the maximum conversion from W to W^* is achieved (peak in W^* profile), and E_{1tot} continues to be increased, the third complex C_3 continues to be produced without being consumed in the fourth reaction (due to insufficient W). This phenomenon is unique to the PAR-i model, and can be controlled by altering the value of $K_d = \frac{d_3}{a_3}$. Indeed, we find that by increasing K_d, we can mitigate this loss in maximum output (see Fig 15). Of course, inhibiting the formation of this complex in this manner also reduces the PAR contribution to the covalent modification cycle.

(c) Unlimited ultrasensitivity is difficult to achieve in complex-complete PAR models

Although ultrasensitive profiles could be obtained for both the PAR-d and the PAR-i models, it is important to consider whether or not the models support *unlimited* ultrasensitivity. In other words, can the slope of the highly sensitive (near-vertical) region of the dose-response profile be made arbitrarily steep in some parameter limit? Unlimited ultrasensitivity is of central importance to the implementation of robust perfect adaptation (RPA), and was incorporated into the influential RPA study by Ma et al. [13] using the Michaelian model discussed in the present work. Since the Michaelian model is capable of achieving unlimited ultrasensitivity in the parameter limit $K_1 \to 0$ and $K_2 \to \infty$ ($K_1 \ll W_{tot} - W^*$ and $K_2 \gg W^*$), we examined the performance of our PAR-d and PAR-i models in this specific parameter regime. As we illustrate in Fig 16 we are unable to achieve unlimited ultrasensitivity using these conditions, for any choice of the remaining parameters in the model. In fact, for both the PAR-d and PAR-i models, as the limits $K_1 \to 0$ and $K_2 \to \infty$ are approached, the system exhibits a steep linear increase in W^* with E_{1tot} close to the origin.

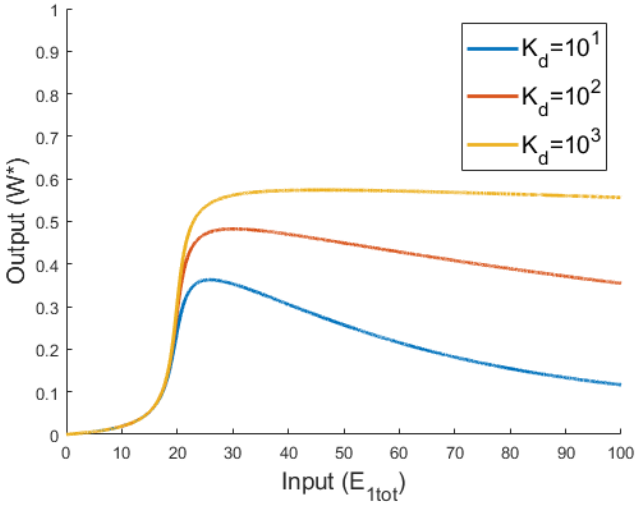

Figure 15. Effect of altering dissociation constant in PAR-i We investigated increasing the value of K_d by decreasing the value of a_3, although the same effect can be created by increasing d_3. We found that by increasing the value of K_d, the maximum abundance of modified substrate increases, and the removal of W^* after this maximum decreases. The parameters used are $W_{tot} = 100$. $E_{2tot} = 20$, $a_1 = d_1 = k_1 = a_2 = d_2 = k_2 = a_4 = d_4 = k_4 = 1$, $d_3 = 10$ with $a_3 = 1$ (blue), $a_3 = 0.1$ (red), and $a_3 = 0.01$ (yellow).

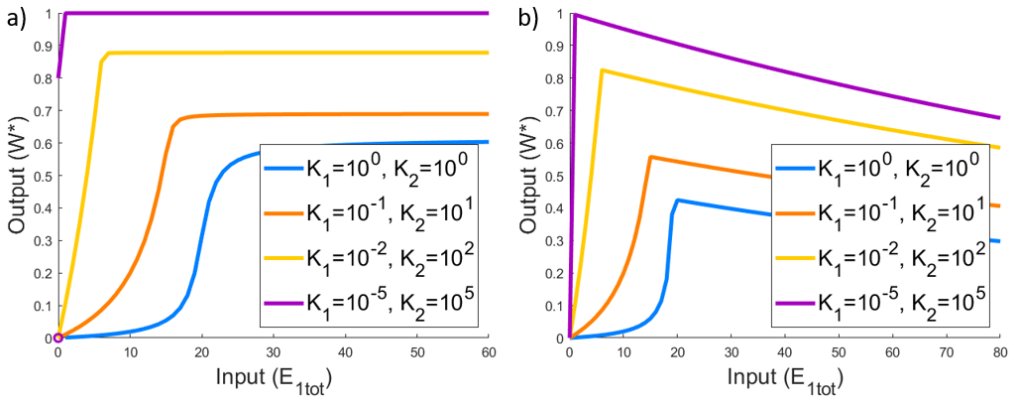

Figure 16. Parameter conditions corresponding to unlimited ultrasensitivity in the Michaelian model, applied to PAR-d and PAR-i In the Michaelian model, unlimited ultrasensitivity obtains in the limit as $K_1 \to 0$ and $K_2 \to \infty$ (ie. $K_1 \ll W_{tot} - W^*$ and $K_2 \gg W^*$). Here we consider the behaviour of the (a) PAR-d and (b) PAR-i models under these parametric conditions. Parameters: $W_{tot} = 100$, $E_{2tot} = 20$, $d_1 = k_1 = d_2 = k_2 = 1$; in addition: $a_1 = 1$, $a_2 = 1$ (blue); $a_1 = 10^{-1}$, $a_2 = 10^1$ (orange); $a_1 = 10^{-2}$, $a_2 = 10^2$ (yellow); $a_1 = 10^{-5}$, $a_2 = 10^5$ (purple). (a) $a_3 = 10^5$, $d_3 = k_3 = 1$, $K_3 = 10^{-5}$; (b) $a_3 = 0.1$, $d_3 = 10$, $a_4 = 10^5$, $d_4 = k_4 = 1$, $K_d = 100$, $K_4 = 10^{-5}$.

Our extensive numerical simulations revealed that the *only* parametric condition that yields unlimited ultrasensitivity in the PAR-d model is $a_3 \to 0$ ($K_3 \to \infty$), along with either $K_1 \to 0$ and $K_2 \to 0$ (Fig 17a) or $W_{tot} \gg E_{2tot}, E_{1tot}$ (Fig 17b). We note that the first of these conditions ($a_3 \to 0$) corresponds to the limit in which the PAR-d mechanism approaches the Goldbeter-Koshland model [46] - ie. a simple covalent-modification cycle *without* positive autoregulation (PAR). In addition, the second set of conditions ($K_1 \to 0$ and $K_2 \to 0$ or $W_{tot} \gg E_{2tot}, E_{1tot}$) corresponds

to parameter regime in which Goldbeter and Koshland [46] achieved unlimited ultrasensitivity via the zero-order mechanism. In other words PAR-d can only exhibit unlimited ultrasensitivity once the PAR contribution is removed. PAR-d, in its essence, appears to be incapable of unlimited ultrasensitivity.

Unlimited ultrasensivity was likewise very difficult to find in PAR-i, although it is possible under very specific conditions. Similar to the situation with PAR-d, unlimited ultrasensitivity may be realised in the parameter limit by which the Goldbeter-Koshland model [46] is recovered from the PAR-i model. This gives rise to dose-response profiles which are identical to Fig 17.

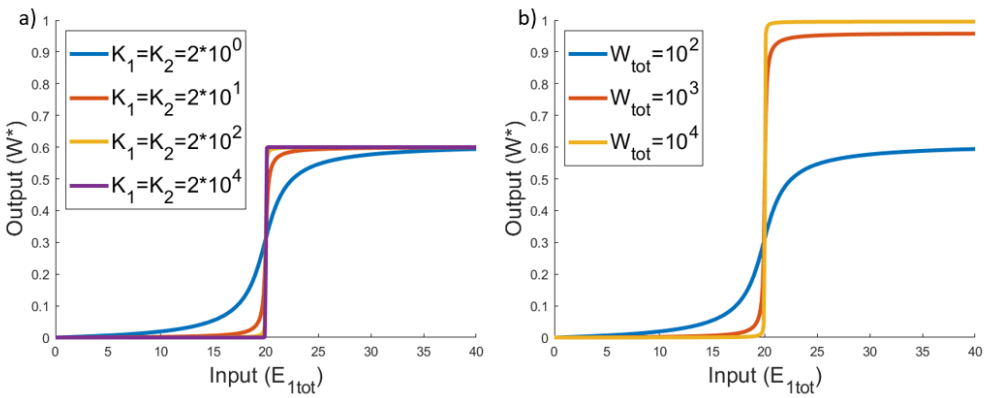

Figure 17. Unlimited Ultrasensitivity in PAR-d Unlimited ultrasensitivity can only obtain in PAR-d in the limit as $a_3 \to 0$, whereby the positive autoregulation is removed from the model, and $K_1,\ K_2 \ll W_{tot}$, which corresponds to the conditions required for zero-order ultrasensitivity. These conditions can be realized by (a) decreasing K_1 and K_2, or (b) increasing W_{tot}. Parameters: $W_{tot} = 100$, $E_{2tot} = 20$, $a_1 = d_1 = k_1 = a_2 = d_2 = k_2 = d_3 = k_3 = 1$, and $a_3 = 10^{-10}$. (a) $a_1 = a_2 = 1$ (blue), $a_1 = a_2 = 10^1$ (red), $a_1 = a_2 = 10^2$ (yellow), and $a_1 = a_2 = 10^4$ (purple); (b) $W_{tot} = 10^2$ (blue), $W_{tot} = 10^3$ (red), and $W_{tot} = 10^4$ (yellow). Almost identical profiles can be achieved in PAR-i by setting $a_3 = 10^{-10}$, $d_3 = 10$, and $a_4 = d_4 = k_4 = 1$ to remove the effect of PAR (not shown).

However PAR-i is also able to create unlimited ultrasensitivity in one additional set of conditions, where PAR remains present in the model. For this, we consistently found that we require $k_1 \approx k_2 \approx k_4$. When this condition holds, unlimited ultrasensitivity may then be achieved by taking the limit as $K_1 \to 0$ and $K_2 \to 0$ (Fig 18a), and/or in the limit as $W_{tot} \to 0$ (Fig 18b).

3. Conclusions

The Michaelis-Menten equation, and variations thereon, has appeared almost ubiquitously in mathematical descriptions of enzyme-mediated chemical reactions for more than 100 years [78,79] - often quite indiscriminately, with little or no consideration of whether it is able to truly recapitulate the behaviour of the (potentially much more complicated) system being modelled. In particular, it has been used in highly-influential work [13] to suggest that positive autoregulation (PAR) of a covalent-modification cycle can generate unlimited ultrasensitivity, and as a consequence, robust perfect adaptation (RPA) when suitably embedded in certain network topologies. Here we ask: Can a Michaelian description of such a system accurately represent the detailed molecular mechanisms that must be present in a 'real' collection of interacting molecules, which could, in principle, be quite intricate and complicated? And can it truly recapitulate the range of qualitative behaviours afforded by more detailed mass-action descriptions that account for all molecular interactions? Our answer, based on two detailed mass-action models which carefully account for the specific molecular mechanisms through which PAR is actually

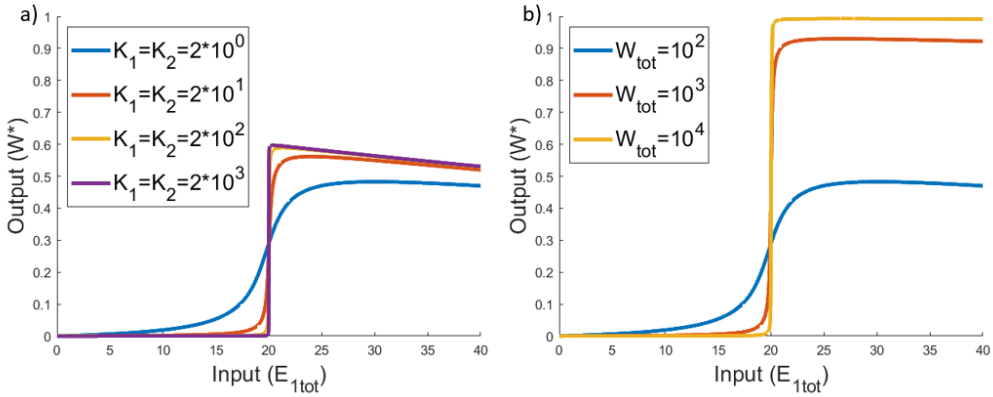

Figure 18. Unlimited Ultrasensitivity in PAR-i In this figure we create conditions on PAR-i under which we can observe unlimited ultrasensitivity without sacrificing the effect of the PAR mechanism. To achieve these plots, we apply the same conditions required for unlimited ultrasensitivity in a reversible covalent-modification cycle as Fig 17. However it is still evident that the PAR mechanism has some effect on the profile, as demonstrated by the distinct decline in modified substrate after the maximum conversion is achieved. A behaviour which is unique to this PAR mechanism. These profiles are achieved by setting $W_{tot} = 100$, $E_{2tot} = 20$, $a_1 = d_1 = k_1 = a_2 = d_2 = k_2 = a_4 = d_4 = k_4 = 1$, $a_3 = 0.1$, and $d_3 = 10$. We then set a) $a_1 = a_2 = 1$ (blue), $a_1 = a_2 = 10^1$ (red), $a_1 = a_2 = 10^2$ (yellow), and $a_1 = a_2 = 10^3$ (purple) and b) $W_{tot} = 10^2$ (blue), $W_{tot} = 10^3$ (red), and $W_{tot} = 10^4$ (yellow)

transacted, and explicitly account for all intermediate molecular species - a framework we call '*complex complete*' - is a resounding *no*.

Although our two complex-complete PAR models (PAR-d and PAR-i) are relatively simple, they exhibit functionally important differences from their Michaelian counterpart, and clearly illustrate that *mechanism matters*. Indeed, although the Michaelian model of PAR has been studied for its capacity to exhibit unlimited ultrasensitivity for the purposes of RPA, we found that our more realistic models that account for the specific mechanism involved were not particularly prone to unlimited ultrasensitivity at all, and required very carefully-orchestrated parametric conditions in order to be able to increase the sensitivities of their dose-response profiles indefinitely. For one of the two mechanisms (PAR-d), unlimited ultrasensitivity could *only* be obtained in the parameter limit corresponding to the complete removal of positive autoregulation from the covalent modification cycle. In any event, neither of our complex-complete models could achieve ultrasensitivity in the parametric circumstances suggested by the Michaelian model (very small Michaelis constant for the 'forward' reaction, and very large Michaelis constant for the 'reverse' reaction).

Both complex-complete PAR models were prone to bistability, however - a qualitative response that is also realised by the Michaelian description. But here again, behaviour of the complex-complete models departs from that of the Michaelian model in significant ways. The PAR-d model - by far the more prone to bistability of the two new models - may readily be shown to exhibit both two-way (reversible) bistable switches *and* one-way (irreversible) switches. Moreover, a full range of qualitative responses - from a monostable ultrasensitive profile, to two-way switches, through to one-way switches - could be generated in the PAR-d model *for a single set of Michaelis constants*, the specific response being determined in each case by *other* component parameters in the model. In contrast, the Michaelis constants alone specify the qualitative nature of the dose-response curve for the Michaelian model. The PAR-i model was shown to be much less prone to bistability than the PAR-d model, and could only exhibit two-way (reversible) switches - a response that is entirely driven by the catalytic rate constant associated with the autoregulatory enzymatic reaction.

Our study suggests that more caution should be exercised in the use of the Michaelis-Menten equation to model enzyme-mediated reactions, particularly in the context of complex signalling networks, and particularly when additional regulations (such as autoregulation) are present. While it is clear that Michaelian models vastly simplify the mathematical analysis of enzyme-mediated reaction networks, where complex-complete models can quickly become very large and complicated, these simpler models can only make useful predictions if they can, in fact, recapitulate the basic qualitative features of their more detailed counterparts.

We note in closing that complex-complete mass-action models, as we propose here, constitute polynomial dynamical systems whose steady-state solutions form algebraic varieties. Significant progress has been made in recent years in the application of Gröbner basis methods to the study of these kinds of models (see for example [80]). Nevertheless, since Gröbner bases can quickly become large and expensive to compute as the underlying models become more complicated, numerical simulations may still be required in many cases to support the analysis of mechanism-based models of complex networks.

4. Methods

Numerical simulations and root finding methods were all undertaken using standard packages available in Matlab (ODE45, ODE23s, roots, and fsolve). Total number of possible steady-states in the interval $[0,W_{tot}]$ were checked by Gröbner basis calculations (and subsequent numerical examination in Matlab) available in the open-source package Singular (https://www.singular.uni-kl.de/). All code available from the authors upon reasonable request.

Data Accessibility. This article has no additional data.

Authors' Contributions. CJS: conceptualization, formal analysis, methodology, software, visualisation, writing- original draft preparation. RPA: conceptualization, methodology, writing – review and editing, supervision.

Competing Interests. We declare we have no competing interests.

Funding. No funding has been received for this article.

Acknowledgements. Robyn P. Araujo is the recipient of an Australian Research Council (ARC) Future Fellowship (project number FT190100645) funded by the Australian Government.

References

1. Shah NA, Sarkar CA. 2011 Robust network topologies for generating switch-like cellular responses. *PLoS Comput Biol* **7**, e1002085.
2. Palani S, Sarkar CA. 2008 Positive receptor feedback during lineage commitment can generate ultrasensitivity to ligand and confer robustness to a bistable switch. *Biophysical journal* **95**, 1575–1589.
3. Ferrell Jr JE. 1999 Building a cellular switch: more lessons from a good egg. *Bioessays* **21**, 866–870.
4. Tyson JJ, Chen KC, Novak B. 2003 Sniffers, buzzers, toggles and blinkers: dynamics of regulatory and signaling pathways in the cell. *Current opinion in cell biology* **15**, 221–231.
5. Araujo RP, Liotta LA, Petricoin EF. 2007 Proteins, drug targets and the mechanisms they control: the simple truth about complex networks. *Nature reviews Drug discovery* **6**, 871–880.
6. Zhang Q, Bhattacharya S, Andersen ME. 2013 Ultrasensitive response motifs: basic amplifiers in molecular signalling networks. *Open biology* **3**, 130031.
7. Shuaib A, Hartwell A, Kiss-Toth E, Holcombe M. 2016 Multi-compartmentalisation in the MAPK signalling pathway contributes to the emergence of oscillatory behaviour and to ultrasensitivity. *PloS one* **11**, e0156139.
8. Montefusco F, Akman OE, Soyer OS, Bates DG. 2016 Ultrasensitive negative feedback control: a natural approach for the design of synthetic controllers. *PloS one* **11**, e0161605.
9. Malleshaiah MK, Shahrezaei V, Swain PS, Michnick SW. 2010 The scaffold protein Ste5 directly controls a switch-like mating decision in yeast. *Nature* **465**, 101–105.

10. Ferrell Jr JE. 1999 Xenopus oocyte maturation: new lessons from a good egg. *Bioessays* **21**, 833–842.
11. Huang CY, Ferrell JE. 1996 Ultrasensitivity in the mitogen-activated protein kinase cascade. *Proceedings of the National Academy of Sciences* **93**, 10078–10083.
12. Melen GJ, Levy S, Barkai N, Shilo BZ. 2005 Threshold responses to morphogen gradients by zero-order ultrasensitivity. *Molecular systems biology* **1**, 2005–0028.
13. Ma W, Trusina A, El-Samad H, Lim WA, Tang C. 2009 Defining network topologies that can achieve biochemical adaptation. *Cell* **138**, 760–773.
14. Araujo RP, Liotta LA. 2018 The topological requirements for robust perfect adaptation in networks of any size. *Nature communications* **9**, 1–12.
15. Araujo RP, Liotta LA. 2020 Design Principles Underlying Robust Perfect Adaptation of Complex Biochemical Networks. *bioRxiv*.
16. Berg HC, Brown DA. 1972 Chemotaxis in Escherichia coli analysed by three-dimensional tracking. *Nature* **239**, 500–504.
17. Macnab RM, Koshland DE. 1972 The gradient-sensing mechanism in bacterial chemotaxis. *Proceedings of the National Academy of Sciences* **69**, 2509–2512.
18. Kirsch ML, Peters PD, Hanlon DW, Kirby JR, Ordal GW. 1993 Chemotactic methylesterase promotes adaptation to high concentrations of attractant in Bacillus subtilis.. *Journal of Biological Chemistry* **268**, 18610–18616.
19. Barkai N, Leibler S. 1997 Robustness in simple biochemical networks. *Nature* **387**, 913–917.
20. Yi TM, Huang Y, Simon MI, Doyle J. 2000 Robust perfect adaptation in bacterial chemotaxis through integral feedback control. *Proceedings of the National Academy of Sciences* **97**, 4649–4653.
21. Mello BA, Tu Y. 2003 Quantitative modeling of sensitivity in bacterial chemotaxis: the role of coupling among different chemoreceptor species. *Proceedings of the National Academy of Sciences* **100**, 8223–8228.
22. Rao CV, Kirby JR, Arkin AP. 2004 Design and diversity in bacterial chemotaxis: a comparative study in Escherichia coli and Bacillus subtilis. *PLoS Biol* **2**, e49.
23. Kollmann M, Løvdok L, Bartholomé K, Timmer J, Sourjik V. 2005 Design principles of a bacterial signalling network. *Nature* **438**, 504–507.
24. Endres RG, Wingreen NS. 2006 Precise adaptation in bacterial chemotaxis through "assistance neighborhoods". *Proceedings of the National Academy of Sciences* **103**, 13040–13044.
25. Parent CA, Devreotes PN. 1999 A cell's sense of direction. *Science* **284**, 765–770.
26. Yang L, Iglesias PA. 2006 Positive feedback may cause the biphasic response observed in the chemoattractant-induced response of Dictyostelium cells. *Systems & control letters* **55**, 329–337.
27. Levchenko A, Iglesias PA. 2002 Models of eukaryotic gradient sensing: application to chemotaxis of amoebae and neutrophils. *Biophysical journal* **82**, 50–63.
28. Reisert J, Matthews HR. 2001 Response properties of isolated mouse olfactory receptor cells. *The Journal of physiology* **530**, 113–122.
29. Matthews HR, Reisert J. 2003 Calcium, the two-faced messenger of olfactory transduction and adaptation. *Current opinion in neurobiology* **13**, 469–475.
30. Hoeller O, Gong D, Weiner OD. 2014 How to understand and outwit adaptation. *Developmental cell* **28**, 607–616.
31. Alon U, Surette MG, Barkai N, Leibler S. 1999 Robustness in bacterial chemotaxis. *Nature* **397**, 168–171.
32. Muzzey D, Gómez-Uribe CA, Mettetal JT, van Oudenaarden A. 2009 A systems-level analysis of perfect adaptation in yeast osmoregulation. *Cell* **138**, 160–171.
33. El-Samad H, Goff J, Khammash M. 2002 Calcium homeostasis and parturient hypocalcemia: an integral feedback perspective. *Journal of theoretical biology* **214**, 17–29.
34. Kaupp UB. 2010 Olfactory signalling in vertebrates and insects: differences and commonalities. *Nature Reviews Neuroscience* **11**, 188–200.
35. Yau KW, Hardie RC. 2009 Phototransduction motifs and variations. *Cell* **139**, 246–264.
36. Ben-Zvi D, Barkai N. 2010 Scaling of morphogen gradients by an expansion-repression integral feedback control. *Proceedings of the National Academy of Sciences* **107**, 6924–6929.
37. Eldar A, Dorfman R, Weiss D, Ashe H, Shilo BZ, Barkai N. 2002 Robustness of the BMP morphogen gradient in Drosophila embryonic patterning. *Nature* **419**, 304–308.
38. Hart Y, Madar D, Yuan J, Bren A, Mayo AE, Rabinowitz JD, Alon U. 2011 Robust control of nitrogen assimilation by a bifunctional enzyme in E. coli. *Molecular cell* **41**, 117–127.
39. Yadid G, Overstreet DH, Zangen A. 2001 Limbic dopaminergic adaptation to a stressful stimulus in a rat model of depression. *Brain research* **896**, 43–47.

40. Medina-Gomez G, Yetukuri L, Velagapudi V, Campbell M, Blount M, Jimenez-Linan M, Ros M, Orešič M, Vidal-Puig A. 2009 Adaptation and failure of pancreatic β cells in murine models with different degrees of metabolic syndrome. *Disease models & mechanisms* **2**, 582–592.
41. Sturgeon JA, Zautra AJ. 2010 Resilience: a new paradigm for adaptation to chronic pain. *Current pain and headache reports* **14**, 105–112.
42. Fodale V, Pierobon M, Liotta L, Petricoin E. 2011 Mechanism of cell adaptation: when and how do cancer cells develop chemoresistance?. *Cancer journal (Sudbury, Mass.)* **17**, 89.
43. Araujo RP, Petricoin EF, Liotta LA. 2007 Mathematical modeling of the cancer cell's control circuitry: paving the way to individualized therapeutic strategies. *Current Signal Transduction Therapy* **2**, 145–155.
44. Geho DH, Petricoin E, Liotta LA, Araujo RP. 2005 Modeling of protein signaling networks in clinical proteomics. In *Cold Spring Harbor symposia on quantitative biology* vol. 70 pp. 517–524. Cold Spring Harbor Laboratory Press.
45. Hill AV. 1913 The combinations of haemoglobin with oxygen and with carbon monoxide. I. *Biochemical Journal* **7**, 471–480.
46. Goldbeter A, Koshland Jr D. 1981 An amplified sensitivity arising from covalent modification in biological systems. *Proceedings of the National Academy of Sciences* **78**, 6840–6844.
47. Ferrell Jr JE, Ha SH. 2014 Ultrasensitivity part I: Michaelian responses and zero-order ultrasensitivity. *Trends in biochemical sciences* **39**, 496–503.
48. Ferrell JE, Ha SH. 2014 Ultrasensitivity part II: multisite phosphorylation, stoichiometric inhibitors, and positive feedback. *Trends in biochemical sciences* **39**, 556–569.
49. Wang M, Weiss M, Simonovic M, Haertinger G, Schrimpf SP, Hengartner MO, von Mering C. 2012 PaxDb, a database of protein abundance averages across all three domains of life. *Molecular & cellular proteomics* **11**, 492–500.
50. Kim SY, Ferrell Jr JE. 2007 Substrate competition as a source of ultrasensitivity in the inactivation of Wee1. *Cell* **128**, 1133–1145.
51. Buchler NE, Cross FR. 2009 Protein sequestration generates a flexible ultrasensitive response in a genetic network. *Molecular systems biology* **5**, 272.
52. Koshland DE, Goldbeter A, Stock JB. 1982 Amplification and adaptation in regulatory and sensory systems. *Science* pp. 220–225.
53. Gardner TS, Cantor CR, Collins JJ. 2000 Construction of a genetic toggle switch in Escherichia coli. *Nature* **403**, 339–342.
54. Ferrell Jr JE. 2002 Self-perpetuating states in signal transduction: positive feedback, double-negative feedback and bistability. *Current opinion in cell biology* **14**, 140–148.
55. Markevich NI, Hoek JB, Kholodenko BN. 2004 Signaling switches and bistability arising from multisite phosphorylation in protein kinase cascades. *The Journal of cell biology* **164**, 353–359.
56. Santillán M, Mackey M, Zeron E. 2007 Origin of bistability in the lac operon. *Biophysical journal* **92**, 3830–3842.
57. Ozbudak EM, Thattai M, Lim HN, Shraiman BI, Van Oudenaarden A. 2004 Multistability in the lactose utilization network of Escherichia coli. *Nature* **427**, 737.
58. Novick A, Weiner M. 1957 Enzyme induction as an all-or-none phenomenon. *Proceedings of the National Academy of Sciences of the United States of America* **43**, 553.
59. Tan C, Marguet P, You L. 2009 Emergent bistability by a growth-modulating positive feedback circuit. *Nature chemical biology* **5**, 842–848.
60. Siegal-Gaskins D, Mejia-Guerra MK, Smith GD, Grotewold E. 2011 Emergence of switch-like behavior in a large family of simple biochemical networks. *PLoS Comput Biol* **7**, e1002039.
61. Huang S, Guo YP, May G, Enver T. 2007 Bifurcation dynamics in lineage-commitment in bipotent progenitor cells. *Developmental biology* **305**, 695–713.
62. Laslo P, Spooner CJ, Warmflash A, Lancki DW, Lee HJ, Sciammas R, Gantner BN, Dinner AR, Singh H. 2006 Multilineage transcriptional priming and determination of alternate hematopoietic cell fates. *Cell* **126**, 755–766.
63. Ferrell JE, Machleder EM. 1998 The biochemical basis of an all-or-none cell fate switch in Xenopus oocytes. *Science* **280**, 895–898.
64. Cross FR, Archambault V, Miller M, Klovstad M. 2002 Testing a mathematical model of the yeast cell cycle. *Molecular biology of the cell* **13**, 52–70.
65. Yao G, Lee TJ, Mori S, Nevins JR, You L. 2008 A bistable Rb–E2F switch underlies the restriction point. *Nature cell biology* **10**, 476–482.
66. Xiong W, Ferrell JE. 2003 A positive-feedback-based bistable 'memory module'that governs a cell fate decision. *Nature* **426**, 460–465.

67. Camperi M, Wang XJ. 1998 A model of visuospatial working memory in prefrontal cortex: recurrent network and cellular bistability. *Journal of computational neuroscience* **5**, 383–405.
68. Ferrell Jr JE, Xiong W. 2001 Bistability in cell signaling: How to make continuous processes discontinuous, and reversible processes irreversible. *Chaos: An Interdisciplinary Journal of Nonlinear Science* **11**, 227–236.
69. Shiraishi T, Matsuyama S, Kitano H. 2010 Large-scale analysis of network bistability for human cancers. *PLoS Comput Biol* **6**, e1000851.
70. Li Y, Li Y, Zhang H, Chen Y. 2011 MicroRNA-mediated positive feedback loop and optimized bistable switch in a cancer network Involving miR-17-92. *PLoS One* **6**, e26302.
71. Tiwari A, Igoshin OA. 2012 Coupling between feedback loops in autoregulatory networks affects bistability range, open-loop gain and switching times. *Physical biology* **9**, 055003.
72. Chickarmane V, Troein C, Nuber UA, Sauro HM, Peterson C. 2006 Transcriptional dynamics of the embryonic stem cell switch. *PLoS Comput Biol* **2**, e123.
73. Ferrell Jr JE. 2002 Self-perpetuating states in signal transduction: positive feedback, double-negative feedback and bistability. *Current opinion in cell biology* **14**, 140–148.
74. Chickarmane V, Enver T, Peterson C. 2009 Computational modeling of the hematopoietic erythroid-myeloid switch reveals insights into cooperativity, priming, and irreversibility. *PLoS Comput Biol* **5**, e1000268.
75. Sabouri-Ghomi M, Ciliberto A, Kar S, Novak B, Tyson JJ. 2008 Antagonism and bistability in protein interaction networks. *Journal of theoretical biology* **250**, 209–218.
76. Feinberg M. 2019 *Foundations of chemical reaction network theory*. Springer.
77. Xing J, Chen J. 2008 The Goldbeter-Koshland switch in the first-order region and its response to dynamic disorder. *PloS one* **3**, e2140.
78. Gunawardena J. 2014 Time-scale separation–Michaelis and Menten's old idea, still bearing fruit. *The FEBS journal* **281**, 473–488.
79. Kim JK, Tyson JJ. 2020 Misuse of the Michaelis–Menten rate law for protein interaction networks and its remedy. *PLoS Computational Biology* **16**, e1008258.
80. Manrai AK, Gunawardena J. 2008 The geometry of multisite phosphorylation. *Biophysical journal* **95**, 5533–5543.